Ion acceleration in the transparent regime and the critical influence of the plasma density scale length

R. A. Loch, T. Ceccotti, F. Quéré, H. George, G. Bonnaud, F. Réau, P. D'Oliveira, M. J. H. Luttikhof, F. Bijkerk, K.-J. Boller, G. Blaclard, and P. Combis

Citation: Physics of Plasmas **23**, 093117 (2016); doi: 10.1063/1.4962571
View online: http://dx.doi.org/10.1063/1.4962571
View Table of Contents: http://scitation.aip.org/content/aip/journal/pop/23/9?ver=pdfcov
Published by the AIP Publishing

Ion acceleration in the transparent regime and the critical influence of the plasma density scale length

R. A. Loch,[1,2] T. Ceccotti,[3] F. Quéré,[3] H. George,[3] G. Bonnaud,[3,4,a)] F. Réau,[3] P. D'Oliveira,[3] M. J. H. Luttikhof,[1] F. Bijkerk,[1,2] K.-J. Boller,[1,2] G. Blaclard,[4] and P. Combis[5]
[1]*Laser Physics and Nonlinear Optics Group, MESA+ Institute for Nanotechnology at the University of Twente, P.O. Box 217, 7500 AE Enschede, The Netherlands*
[2]*FOM-Institute DIFFER – Dutch Institute for Fundamental Energy Research, P.O. Box 1207, 3430 BE Nieuwegein, The Netherlands*
[3]*LIDYL, CEA, CNRS, Université Paris-Saclay, CEA Saclay, 91191 Gif-sur-Yvette, France*
[4]*INSTN, CEA Saclay, Université Paris-Saclay, 91191 Gif-sur-Yvette, France*
[5]*DPTA, CEA DIF, 91297 Arpajon Cedex, France*

(Received 26 April 2016; accepted 29 August 2016; published online 21 September 2016)

The influence of a plasma density gradient on ions accelerated along the specular (back reflection) direction in the transparent Target Normal Sheath Acceleration regime is investigated. Enhanced acceleration of ions is experimentally observed in this regime using high-intensity and ultra-high contrast laser pulses and extremely thin foils of few nanometer thicknesses. The experimental trend for the maximum proton energy appeared quite different from the already published numerical results in this regime where an infinitely steep plasma gradient was assumed. We showed that for a realistic modelling, a finite density gradient has to be taken into account. By means of particle-in-cell (PIC) simulations, we studied for the first time the influence of the plasma density scale length on ion acceleration from these nanofoil targets. Through a qualitative agreement between our numerical particle-in-cell simulations and our experiments, the main conclusion with regard to the experimental requirements is that, in the transparent regime evidenced with nanofoils as compared to the opaque regime, the plasma expansion has to be taken into account and both the pulse contrast and the damage threshold of the material are essential parameters. *Published by AIP Publishing.*
[http://dx.doi.org/10.1063/1.4962571]

I. INTRODUCTION

Laser-driven ion beams offer a combination of attractive physical properties, including high brightness, low transverse divergence, a high laminarity, multi-MeV energies, and an ultrashort duration. These properties make these ion beams very promising, e.g., radiography, isotope production for positron emission tomography (PET) scanners, high-brightness injectors for accelerators, proton imaging, and cancer therapy, provided that the ion flux and energy is increased with regard to what is available today at a high repetition rate.[1]

Ultra-high contrast laser pulses presently allow to explore the relativistic regime of ion acceleration using extremely thin foils, with thicknesses in the order of the penetration depth of the laser light. Numerical calculations predict that in this so-called transparent regime, the flux and maximum energy of ions would increase due to the increase in the temperature and density of hot electrons.[2,3] However, this prediction relies on the standard assumption of a plasma density distribution starting with an infinitely steep gradient, neglecting the important physical effects of the early expansion of the plasma before the drive pulse reaches its peak intensity.

In this paper, we study the influence of the plasma density scale length on the maximum energy of backward accelerated protons in the transparent regime. For the sake of clarity, throughout this paper, we shall use the term "backward" for ions accelerated along the specular direction, that is, opposite to the incoming laser direction and escaping the target through their front (illuminated) side. By contrast, the term "forward" qualifies the ions going along the same direction than the laser one and escaping the target through their back side. The motivation for this research is to allow a comparison with the previously mentioned calculations using the standard, barely physical, approach of an infinitely steep gradient (as generally assumed in numerical calculations for ultra-high contrast laser pulses), and to identify the actual laser and target requirements for most advantageous output of proton acceleration. We performed numerical calculations using plasma density ramps and compared the results with experiments on ion acceleration in the transparent regime by exploiting the thinnest foils till date. We show that for a realistic modelling of ion acceleration in the transparent regime, a plasma gradient has to be considered, even when using ultra-high contrast laser pulses.

The acceleration of protons and ions from solid foil targets has initially believed to depend on standard parameters of the laser pulse, such as the peak intensity, the pulse duration, the polarization, and the angle of incidence of the light, as well as the target thickness and maximum density.[4] It is also known that, especially for decreasing foil thicknesses, a central problem is the plasma density profile which relates to the temporal contrast of the pulse, as pre-pulses or the pedestal of very intense beams can be strong enough to induce an

a)E-mail: guy.bonnaud@cea.fr

undesired, premature plasma expansion that hinders the interaction of the laser pulse with a high-density plasma. The pulse contrast available with standard chirped pulse amplification (CPA) laser systems (usually about 10^6 to 10^9) can be nonetheless improved by orders of magnitude by employing contrast enhancement techniques like double plasma mirrors (DPMs).[5,6] Such high-contrast pulses, particularly when using thin foils as targets (50 nm to several micrometers), resulted in high-energy accelerated protons and ions emitted from both sides of the foil,[7–13] in good agreement with the well-known Target Normal Sheath Acceleration (TNSA) mechanism.[14,15] These results have led to the general belief that premature plasma expansion is negligible when using ultrahigh-contrast laser pulses, which seems valid for the opaque regime of TNSA. The onset and influence of preplasma formation, however, also depends on the target thickness and damage threshold.

Previously, we reported on ion acceleration via TNSA from extremely thin foils down to 1 nm, thereby entering the transparent regime experimentally for the first time.[16] We observed an enhanced backward acceleration of ions from foils having thicknesses in the order of the penetration depth of the laser light. Using thinner and thinner foils, first we observed the expected decrease of maximum proton energy below the optimum thickness,[8,10,11,17] which is then followed by a re-increase of the proton energy, like in Ref. 18. This trend, however, deviates from the theoretical prediction in the transparent regime. Our results suggested that, even with ultra-high contrast laser pulses, a plasma is formed with a density gradient that is large enough to be taken into account. Here, we go beyond all previous attempts, using higher laser intensities and systematically investigate the effect of a small, non-zero plasma gradient on the ion acceleration in the transparent TNSA regime.

Our analysis will be divided as follows. In Sec. II, we shall present a description of the set-up used in the experiments and report on the experimental observations. Section III will be devoted to the simulations of the interaction of the main laser pulse with ultra-high intensity and subpicosecond duration with a plasma, with both a compendium of parameters used in the numerical calculations and the numerical observations. Section IV is concerned with the target behavior when impinged by a long nanosecond–low intensity laser prepulse. Finally, our conclusions are gathered in Sec. V.

II. EXPERIMENTAL SET-UP AND OBSERVATIONS

The experiment was performed with the 100 TW laser (UHI 100) at the Saclay Laser-matter Interaction Center (SLIC) in CEA-Saclay. The laser delivers 2.2 J pulses compressed to 25 fs at a central wavelength $\lambda = 800$ nm. The laser pulse coming from the compressor was cleaned from amplified spontaneous emission (ASE) and the pedestal to achieve an ultra-high pulse contrast using a DPM before entering the interaction chamber. The pulse contrast, measured with a Sequoia third-order autocorrelator, on the nanosecond time scale was 10^{12} after the DPM as compared to a contrast of 10^9 before temporal cleaning.[19] With the DPM, the temporal profile of the laser pulse exhibits a very fast rising edge of about 12 orders of magnitude in less than 1 ps. The pulse was focused on the target with a 300 mm focal length off-axis parabolic mirror (OAP), under an angle of 45° in p-polarization to a spot size of approx. 5 to 10 μm FWHM. The resulting estimated focused intensities were about a few 10^{19} W/cm^2. We used mono-polymer polystyrene plastic and carbon foils as a source for protons and ions. The target orientation was verified using a laser beam pencil co-propagating all along the pump beam path and a small mirror mounted on the holder. The precision in tilt and rotation we get in this way was better than 0.1°. The exact position of each foil along the focusing parabola optical path was then verified superposing two other small laser beam pencil spots on the target (which were real time imaged on a CCD) once the latter lies at the optimal position (i.e., the one corresponding to the maximum proton energy). With the two pencils impinging on the target with a large angle (>45°), any eventual foil shift from its position leads to a shift of the two pencil spots and allows us to put the target back to the right position. The precision we obtained in this way was better than 50 μm, to be compared to the focusing confocal parameter that was of the order of 150 μm.

Ion and proton spectra were recorded with a Thomson parabola ion spectrometer (TP) followed by a two-stage, 40 mm-diameter microchannel plate (MCP) coupled to a phosphor screen, which was imaged onto a 12 bit CCD camera. The TP entrance pin-hole diameter was 150 μm. Due to the source-to-pin-hole and pin-hole-to-detector distances ratio, the spatial (energy) resolution was about 270 μm (about ±0.15 MeV for cut-off energies between 4 and 6 MeV). We deeply saturated the MCP signals in order to easily detect even the weakest signal corresponding to the high energy spectral distribution tail. The uncertainty that is specific to this method is of the same order of the diagnostic intrinsic one. This detection unit was pointed towards the target in the direction normal to the irradiated surface of the target to characterize particle acceleration in the backward direction. The ion traces were analyzed for the maximum energy, using the commercial code SIMION.[11]

In order to compare the data between the carbon and polystyrene foils, in Fig. 1, the measured maximum proton energy is plotted as a function of the foil areal density (open circle and triangle symbols, respectively). Carbon nanofoils with an areal density of 0.4 to 14.3 μg/cm^2 have been used, corresponding to thicknesses of, successively, 2, 7, 11, 19, 27.5, 35, 50, and 71.5 nm. The mass density of arc-evaporated carbon foils with an areal density larger than 0.5 μg/cm^2 is 2.01 ± 0.02 g/cm^3, and the density is 1.8 g/cm^3 for foils of 0.5 μg/cm^2 and lower.[20,21] Plastic polystyrene foils of 100, 200, 400, and 800 nm thicknesses have been irradiated with the laser pulses as well. The mass density of these foils is 1.05 g/cm^3. As can be seen in Fig. 1, the average values of the maximum proton energy at 10 μg/cm^2 for carbon and polystyrene are very similar.

The maximum proton energy as a function of the foil thickness shows a more or less constant value around 5.8 ± 0.8 MeV. However, inspecting the trend of the data in Fig. 1 in more detail moving from thicker to thinner foils, an increase in the maximum proton energy can be seen down to

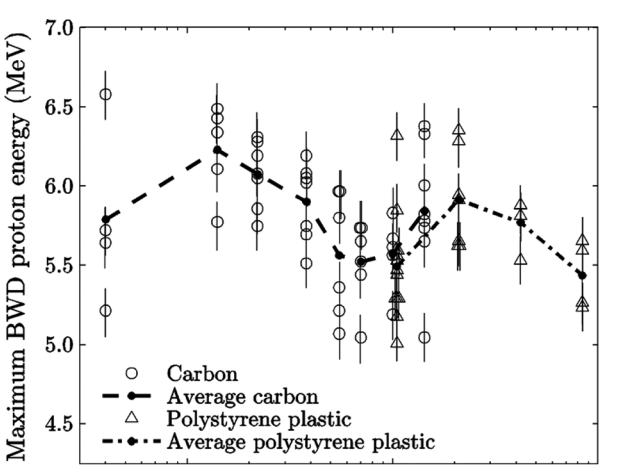

FIG. 1. Maximum proton energy observed in the backward direction (BWD) normal to the target, using carbon (open circles) and polystyrene (open triangles) targets. The experimental error of each data point was about 0.3 MeV (full width). For a better display of separate data points, overlapping points have been slightly shifted in areal density. The filled dots are the average values for each areal density value. The lines are a guide for the eye.

the first peak at around 20 μg/cm^2. This can be explained by the enhancement of the electron temperature due to recirculation of the electrons.[8,22,23] Below 20 μg/cm^2, the maximum energy drops. We interpret this as the result of a shock wave, induced by the pedestal of the laser pulse causing the expansion of the complete foil before the main pulse arrives, as described in Refs. 8, 22, and 23. This trend appears to persist down to an areal density of 7 μg/cm^2, corresponding to about 35 nm thick carbon. For extremely thin carbon foils of a few nanometers thick (corresponding to around 1 μg/cm^2), one can observe a second peak in the maximum proton energy slightly higher than the first peak.

These experimental results appear quite different from the theoretically predicted curve[2,3] for ion acceleration in the transparent TNSA regime based on the standard assumption of a step-like plasma density profiles. Our novel experimental data in the transparent regime point out that a better physical picture and, subsequently, an improved theoretical description are required.

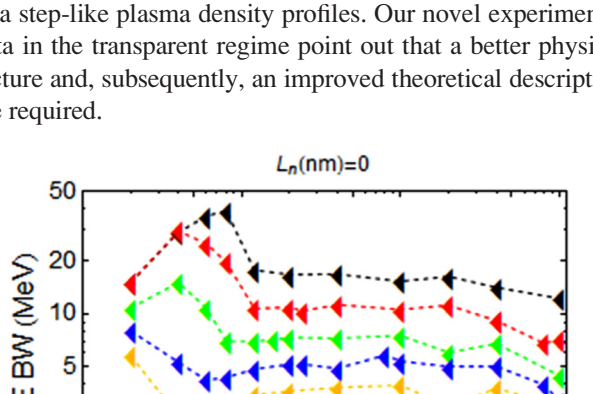

FIG. 2. Calculated dependency of the maximum proton energy in the backward direction on the foil thicknesses. The initial plasma density is assumed to have a standard, step-like profile ($L_n = 0$), which neglects the pre-expansion of foils. From bottom to top, $a_0 = 0.75, 1.25, 1.77, 2.5, 3.54, 5$.

III. SIMULATIONS OF THE INTERACTION OF THE ULTRAHIGH INTENSITY—SHORT LASER PULSE WITH THE TARGET PLASMA

We suggest that the main parameter to take into account is the finite scale length density gradient of the plasma. Without delving too far in the explanations which are gathered in Sec. IV, we can anticipate that the target can be heated by the laser prepulse up to, say, 1000 K, and transformed into gas. As a result, the target illuminated surface will expand with typical velocity $\sqrt{p/\rho}$ (with p the pressure and ρ the target density) that is roughly 1000 m/s; during one nanosecond, the target gas puff will extend up to 10^3 nm. As the target is not immediately heated, we have chosen to use a large set of target expansion sizes between 0 and 10^3 nm, assuming transformation into a plasma during the very beginning of the main laser pulse.

A large set of particle-in-cell (PIC) simulations have been carried out within 1D geometry by using the EUTERPE code, which features the capacity to model oblique incidence.[24,25] Oblique incidence with angle θ is indeed caught by performing simulations in a mobile frame with transverse drift velocity $v_d = c \sin\theta$, in which the plasma electrons and ions, initially immobile in the lab frame, drift along the opposite direction $-v_d$. c stands for the velocity of light in vacuum. By this technique, transverse oblique incidence waves can be correctly modelled, and whatever the waves can be considered as plane waves, the physics of laser-plasma interactions can be correctly reproduced.[25] To make sure the simulation runs respect the physics, we have tested the influence of the mesh discretization size and the number of macroparticles. Aware of the fact that both initial plasma size as short as 2 nm and plasma expansion had to be correctly framed avoiding ions to reach the simulation box boundaries, it appears that the cell size $\Delta x = 2\pi/400\, c/\omega_0$ (ω_0 denotes the laser-wave radial frequency) allows convergence of the simulation results; larger cells depart from the lower size results inasmuch as the size is large and smaller cells do not bring any advantage. As Maxwell equations were solved with an explicit scheme, we used for stability a Courant-Friedrichs-Levy (CFL) ratio equal to unity, the latter defined $CFL = c\Delta t/\Delta x_{code}$ in the simulation frame in which actually the mesh size is $\Delta x_{code} = \Delta x/\gamma_d$ with γ_d the Lorentz factor $1/\sqrt{1-(v_d/c)^2}$. We chose $CFL = 1$ that means we imposed $c\Delta t = \Delta x/\sqrt{2}$. As to the number of macro particles, 10^5 macroparticles have been used per species, but no substantial modification was observed by decreasing that number to 2×10^4 macroparticles. A 4-node scheme was used for field interpolation from mesh nodes to macroparticle locations and macro particle charge/current assignation to mesh nodes. All the simulations have been run over 2000 ω_0^{-1}, i.e., 849 fs for 0.8 μm laser wavelength; this time has been observed to be required and sufficient to make ion acceleration be completed even for the larger laser irradiance runs. The plasma slab had its central point located at the box center and surrounded by 3×10^5 meshes of vacuum; 1.8×10^5 time steps have been used.

In order to investigate the effect of a non-zero plasma density scale length on the interaction of the laser pulse and

the maximum proton energy, because the exact density scale length in experiments is unknown, we performed calculations with differently expanded plasmas and compared this with the experimental results and the predicted trend of the transparent TNSA regime. First, to confirm that an enhanced peak in the maximum proton energy is observed with our used laser parameters, and also to check if our calculations are consistent with already published numerical results,[2,3] we performed calculations for several foil thicknesses using plasma profiles with an infinitely steep gradient. Second, different short density scale lengths (up to $L_n/\lambda = 1$, where Brunel absorption and $\mathbf{v} \times \mathbf{B}$ heating are the dominating heating mechanisms[11,26]) were used in numerical modelling with foils featuring initially a density ramp with an exponential profile on the illuminated side of the thin foil.

We have considered three different quantities as parameters. So, we have simulated 11 different target thicknesses, with for each 9 different density ramps and at last for each 6 distinct irradiances in the interval [1.2, 53] 10^{18} W/cm^2 associated with $a_0 = 0.75$, 1.25, 1.77, 2.5, 3.54, 5, that is a set 594 simulations, keeping the same numerical conditions. a_0 stands for the normalized electric field $eE_0/(m_e\omega_0 c)$; e and m_e denote the electron charge and mass, respectively. Roughly 4.2 h were required to complete one simulation on one single processing core of a mesoscale high performance computer server featuring 92 16-core processors with Intel Fortran. Same runs executed on Lenovo 4 core processors with GNU Fortran took 2.3 folded wall clock computer time to complete. Up to 48 simulations could be carried out simultaneously on the computer server. As a diagnostic to test the right run of the simulations, we have checked that the laser absorption measured either by fields only or by macroparticles only did not differ by more than 0.02%–0.2%, excluding the undesired self-heating and so ensuring the quality of the PIC simulations.[27] The plasma was composed by a mix of H^+ and C^{6+} ions with charge densities 14 and 154 n_c mocking the polystyrene C_8H_8 makeup. The initial electron density was 168 n_c to create a neutral plasma with zero electric field at initial time. The laser electric field was bell shaped with profile $a_0(\sin \pi t/\tau)$ if $0 \le t \le \tau$ and 0 outside, with full width $\tau = 120\omega_0^{-1}$, i.e., 25 fs FWHM duration. The maximum energy along the backward direction was extracted from the proton phase space.

The standard results based on the assumption of an initially infinitely steep plasma gradient, thus neglecting the pre-expansion of the ionized foils, are shown in Fig. 2. The bulk target is associated with the right side of the graph.

When comparing the numerical data as shown in Fig. 2 to the results reported in Refs. 2 and 3, it can be concluded that the trends of the maximum proton energy are indeed very similar. Our calculations also clearly show the enhanced peak in the transparent regime of TNSA, for foils thickness around 10 nm under our conditions. In accordance with the descriptions of Dong and d'Humieres,[2,3] the maximum energy shows a strong decay on both sides of the optimum thickness and a weaker decay towards thicker foils in the opaque regime. As can further be seen in Fig. 2, the peak value of the maximum energy of the accelerated protons in the transparent regime is approximately twice as high as the maximum energy at the transition to the opaque regime. Actually, for all foil thicknesses, the maximum proton energy in the backward direction is somewhat smaller than in the forward direction. We attribute this to the small additional expansion during the main laser pulse interaction at the front surface, consistent with previously reported numerical calculations and experimental observations.[11]

However, when comparing the curve in Fig. 2 with the experimental data in Fig. 1, we observe a dissimilar trend. For a further insight of this observation, we took into account the pre-expansion of the plasma in the following set of calculations on the maximum proton energy and investigated in more detail the influence of the plasma density scale length for the various foil thicknesses of interest.

If we take into account the presence of a plasma with different density scale lengths as illustrated in Fig. 3, we observe that the proton energy is clearly the highest for the thinnest foils which correspond to the transparent regime (<20 nm). However, there is a strong dependence on the density scale length: a strong decrease in the maximum proton energy is observed when increasing the density scale length. This means that extremely thin foils, in the transparent regime, are indeed the preferred choice for generating the highest proton energies, but this advantage can only be gained with a sufficiently high contrast of the laser. On the contrary, foils in the opaque regime (>20 nm) are hardly sensitive to the short density scale lengths considered in these numerical calculations. This observation is consistent with the general belief that with ultra-high contrast laser pulses the effect of pre-plasma is negligible on ion acceleration when using thick opaque targets. This robustness seems like a practical advantage in terms of more convenient laser specifications; however, it also means that the proton energy could have been more than a factor of 2 higher with the same drive laser pulse. Actually, the enhancement that can be achieved by moving into the transparent regime diminishes with increasing the density scale length, and the trend of the maximum proton energy versus the foil thickness flattens. Energies are increased by lengthening the density ramp: the values measured for $L_n = 800$ nm ramp profile are 25% higher than for 80 nm ramp.

The flattened curve for the maximum proton energy obtained with the relatively large density scale length is qualitatively in agreement with our experimental data in Fig. 1 and suggests the presence of a plasma gradient formed by the pedestal of the ultra-high contrast laser pulse with the density scale length $L_n = 80$ nm, i.e., $L_n/\lambda = 0.1$. This similarity between the numerical and the experimental results becomes even better evidenced when the maximum proton energy in the backward direction is plotted as a function of the foil thickness, with the average values of the experimental data of Fig. 1, as shown in Fig. 4. Two bumps can be seen: one bump in the opaque regime for thicker foils and one peak at foil thicknesses corresponding to the transparent TNSA regime.

Simulations have been performed by adding an exponential profile on the not illuminated side of the foil as well. Whereas a $L_n = 80$ nm density scale length for the one side exponential profile is required to make the energy peak disappear, a $L_n = 40$ nm length is sufficient for a two side

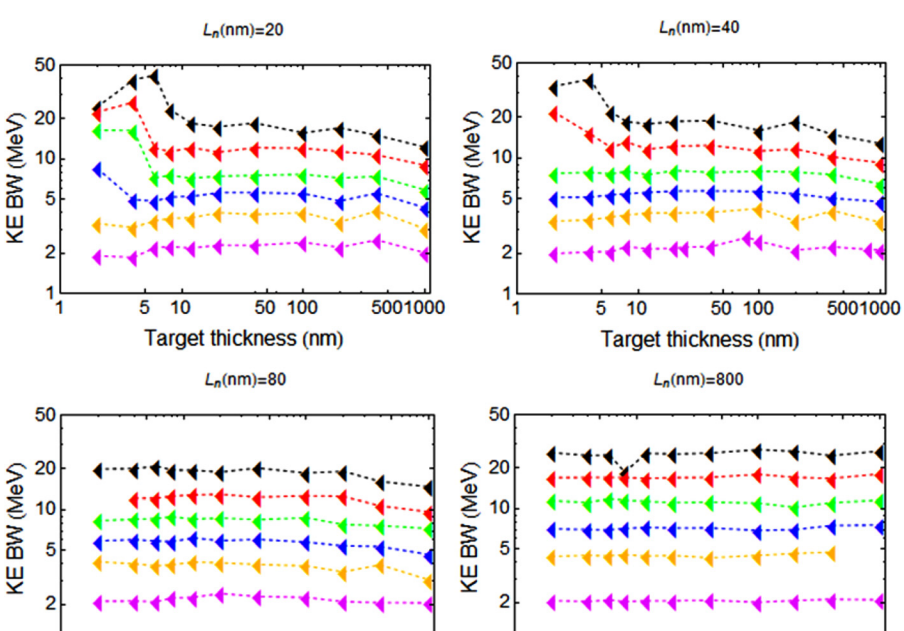

FIG. 3. Calculated dependency of the maximum proton energy on the foil thickness for different plasma density scale lengths L_n. From bottom to top, $a_0 = 0.75, 1.25, 1.77, 2.5, 3.54, 5$.

expansion with the exponential profile. For thick targets (>100 nm), adding a density ramp on the rear surface of the target has no effect on the ions accelerated in the backward direction (which we are mainly interested in) and decreases the maximum energy in the forward direction with at most 20%.[13] Therefore, taking into consideration, a two-sided expansion does not modify our initial conclusion and shows that the large set of results obtained with the one side exponential profile give quantitatively how the energies are influenced.

IV. SIMULATIONS OF THE INTERACTION OF THE LOW INTENSITY—LONG LASER PREPULSE WITH THE SOLID TARGET

Unfortunately, the damage threshold of a few nanometers thick freestanding carbon foil is unknown. Furthermore, it depends on the laser pulse duration and on the target thickness. There is a large range of known damage thresholds of carbon: bulk carbon or graphite has a damage threshold of about 10^7 to 10^9 W/cm^2 for nanosecond pulses,[28,29] while carbon films on a thick substrate have a damage threshold of 10^{12} W/cm^2 for femtosecond pulses.[30] In addition, the damage threshold can decrease by more than an order of magnitude for submicrometer thicknesses as compared to bulk targets.[31] In addition, since we use extremely thin foils, heat conduction is confined to two dimensions (instead of three in bulk targets) which further could lower the damage threshold of the carbon nanofoils for irradiation on the picosecond and nanosecond time scale. Obviously, a higher damage threshold results in a shorter density scale length formed by the laser pedestal. In our quest of quantitative results at low laser irradiance, we found in Ref. 32 a report on an aluminum target illuminated by a 10^{11} W/cm^2 laser prepulse and its dynamics compared to the dynamics of the same target protected by a carbon foil located at 0.5 μm in front of the illuminated side. Unfortunately, the laser prepulse level was too much large compared to the prepulse level in our experiment.

To know the behavior of the target illuminated by a low intensity–long duration prepulse, we have performed simulations with the code ESTHER[33,34] which is able to manage the four states of matter within a hydrodynamic model.

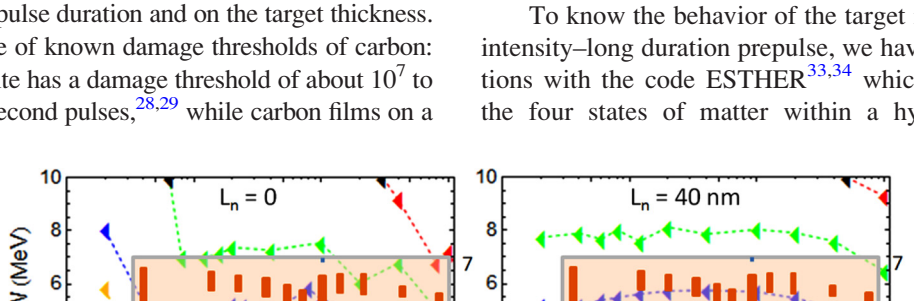

FIG. 4. Comparison between experimental and calculated values of the maximum proton energy in the backward direction as a function of the plasma thickness. Triangles and the left y-axis correspond to numerical calculations where the initial plasma profile has a density scale length L_n = (left) 0 and (right) 40 nm (as in (f)). The vertical bars and the right y-axis correspond to the average values of the experimental data of Fig. 1. From bottom to top, $a_0 = 0.75, 1.25, 1.77, 2.5, 3.54$, the $a_0 = 5$ case is above the displayed frame.

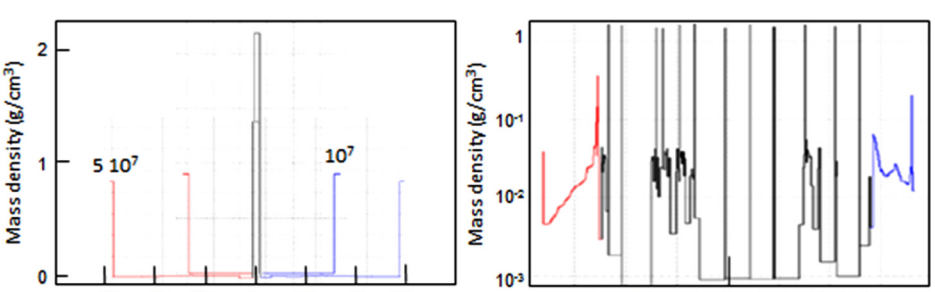

FIG. 5. Mass density profile of the HCH sandwich target (2 nm thickness each) after 1 ns of a constant prepulse irradiance 10^7, 5×10^7 (left), 10^8 (right) W/cm^2. Simulations from ESTHER code. Colours are associated with the target material: illuminated-side water slice in red, carbon in black, and non-illuminated water slice in blue.

Figure 5 displays the typical pattern of the mass density profile. Carbon–hydrogen (CH) made targets and heterogeneous HCH targets, looking as a sandwich of two pollution H (water) slices framing a carbon slice, have been simulated with thickness and laser prepulse intensity as parameters. For 10^7 W/cm^2 irradiance, CH does not show any modification; the target is indeed transparent and does not absorb light. Conversely, the HCH target shows light absorption in the carbon slice which is opaque to light and a subsequent temperature increase of the carbon slice. As a result, H is vaporized on the inner side at the CH interface and the H vapor pushes outside the remaining H slice. After 1 ns, for a very thin target (2 nm thickness), we can observe the target to show a fence pattern with a carbon slice surrounded by 2 hydrogen slices and in between a very low density Hydrogen vapor. For very thin carbon slices (a few nanometers), symmetry around the carbon slice is observed; by contrast, if the carbon thickness is in excess of 100 nm, time delay is observed for heat diffusion from the illuminated side to the opposite one and the hydrogen removal from the target expansion loses its symmetry. In this condition, only the illuminated side is modified before the main pulse reaches the target surface. This picket fence target profile is observed, whereas the pedestal irradiance stays below 10^8 W/cm^2. For irradiances above 10^8 W/cm^2, the carbon slice appears to explode in association with a carbon temperature in excess of 6000 K. The time when this temperature is reached goes down: 0.6 ns, 0.25 ns, and 0.1 ns for irradiances 10^8, 3×10^8, and 10^9 W/cm^2. Once this temperature is reached, the carbon foil becomes an aerosol composed with initial density droplets showing multiple peaks of densities as shown in Fig. 5. At 6×10^8 W/cm^2, the 2 nm thick target is exploded and expanded up to 300 nm.

On the basis of analytical solutions of the heat equation, we can enlighten the physical process underlying this scenario. The solid target dynamics is driven by heat diffusion along the carbon slice. If the quantity D stands for the carbon thermal diffusivity (m^2/s), κ the carbon thermal conductivity (W/m/K), t_p the prepulse duration, and I_p the prepulse irradiance, the temperature reached on the illuminated side reads $T_{in} + I_p/k\sqrt{4Dt_p}$. T_{in} refers to the initial room temperature. We assume full absorption by carbon of the incident laser flux. The deposited heat diffuses down to the non-illuminated side. If the slice thickness ℓ is such that $l/\sqrt{4Dt_p} < 1$, the rear side temperature is close to the illuminated face range and the slice is candidate to explode symmetrically. Otherwise, the rear part of the carbon slice will keep its initial density, and an exponential density profile can be expected on the carbon slice front. The typical carbon extension length is $c_s(t\text{-}t_{ex})$, where t_{ex} stands for the time when the target temperature reaches $T_{ex} = 6000$ K provided by $t_{ex} = \sqrt{KT_{ex}/m_c}\sqrt{(T_{ex} - T_{in})k/I_p/(4D)}$. K denotes the Boltzmann constant, and m_C is the carbon atom mass. Using the plausible values for the carbon thermal features provides the orders of magnitude of the target temperatures and exploded target size provided by the code ESTHER when the 1 ns prepulse phase ends. In contrast to the 1D reported ESTHER simulations showing permanent ordering of the separated fluid water and carbon slabs, realistic 3D geometry behavior will certainly show carbon and hydrogen mixing. We speculate with confidence that with very thin targets the main pulse will interact with a low density CH liquid-gas target. This is why we chose in the PIC simulations to initialize a plasma with a continuous density ramp. More investigation is required to get a better knowledge of the profile and structure of the target when impinged upon by the main pulse and to gauge the impact on proton acceleration of its density profile pattern among picket fence, uniform low density, and separated or mixed carbon and hydrogen. This demanding analysis will be addressed in a future paper.

V. CONCLUSIONS

We want to stress that the proton kinetic energies extracted in the simulations (Figs. 2 and 3) stay above the experimental values (Fig. 1) by a factor of 2 at least. The results from a 2D PIC code by Lefebvre *et al.*[35] report kinetic energies in the range of [4–5.5] MeV for $a_0 = 2$, instead of 6 MeV observed in our 1D simulation results. Like in Antici *et al.*,[26] the 1D geometry impedes any transverse spreading of the electron cloud within the target and in vacuum, and thus, the accelerating field strength is overestimated. As the energies are proportional to the hot electron density, we can assert that the density in a more realistic 2D and 3D geometry would be twice smaller as that in the 1D simulations. But this feature of the 1D simulations is not so clear for large irradiances (10^{20} W/cm^2) as in Ref. 36 where 1D PIC simulations provide good agreement with the experimental values obtained on Trident Laser.

Matching experimental and PIC results reported herein allow us to contemplate two options: (i) assuming that 1D PIC simulations are realistic both qualitatively and quantitatively and that no expansion is induced by the prepulse ($L_n = 0$) make us conclude that the experimental peak irradiance in the main pulse was $I_m/8 = 7 \times 10^{18}$ W/cm^2; (ii) assuming that 1D simulations overestimate the proton kinetic

energy by a factor of 2, only due to 2D/3D electron expansion, and the subsequent electron density and electrostatic potential reduction, and that the experimental irradiance was $I_m/2 = 3 \times 10^{19}$ W/cm^2 make us infer that the laser prepulse has induced expansion with typical density scale length 70 nm, consistent with the ESTHER simulations. The first option cannot be supported since it would mean that the irradiance control was very poor; the experimentalists can accept that not perfectly controlled aberrations have reduced the peak irradiance by a factor of 2 but not by a factor of 8. The second concluding option can be supported in coherence with the computer observations.

To conclude, we performed PIC simulations on ion acceleration in the transparent Target Normal Sheath Acceleration (TNSA) regime that takes into account the limited expansion of the foils caused by a finite pulse contrast. They show that very thin foils, within the nanometer thickness range, lead to the highest maximum proton energies in the so-called transparent TNSA regime. To reach this regime, it seems qualitatively known that a high pulse contrast is of importance when specifying the properties of a laser system. Our comparative analysis between the experimental data and PIC simulation results is the first quantification of such kind. We showed that for the opaque regime, a small density scale length ($L_n/\lambda < 0.1$) indeed has hardly any influence on the maximum proton energy. However, the enhancement of the maximum proton energy with foils in the transparent regime does require a rather small density scale length, i.e., an almost step-like plasma profile in numerical calculations. Increasing the plasma density scale length, resulting in a flattening of the trend for moderate density scale lengths, i.e., $L_n/\lambda > 0.04$ (resp. 0.08) for peak irradiance below 10^{19} (resp. as large as 5×10^{19}) W/cm^2, dims the advantage of ion acceleration in the transparent regime over the opaque regime. To make use of the important potential of the transparent regime, our investigations prove clearly that to reduce the pre-expansion, further progress has to be made with respect to the laser pulse parameters (extremely high pulse contrast) or to the target, by developing freestanding nanofoils with a higher damage threshold than amorphous carbon, such as silica, Mylar, or diamond-like carbon.[31]

ACKNOWLEDGMENTS

This work was financially supported by the Dutch Ministry of Education, Culture, and Science (OC&W), by Laserlab Europe and by the Conseil Général de l'Essonne (ASTRE program). G.B. acknowledges interesting discussion with Dr. O. Rosmej on low intensity laser-solid interactions.

[1]A. Macchi, M. Borghesi, and M. Passoni, Rev. Mod. Phys. **85**, 751 (2013), and references therein.
[2]Q. L. Dong, Z.-M. Sheng, M. Y. Yu, and J. Zhang, Phys. Rev. E **68**, 026408 (2003).
[3]E. D'Humières, E. Lefebvre, L. Gremillet, and V. Malka, Phys. Plasmas **12**, 062704 (2005).
[4]P. Gibbon and E. Forster, Plasma Phys. Controlled Fusion **38**, 769 (1996).
[5]G. Doumy, F. Quéré, O. Gobert, M. Perdrix, Ph. Martin, P. Audebert, J. C. Gauthier, J.-P. Geindre, and T. Wittmann, Phys. Rev. E **69**, 026402 (2004).
[6]A. Lévy, T. Ceccotti, P. D'Oliveira, F. Réau, M. Perdrix, F. Quéré, P. Monot, M. Bougeard, H. Lagadec, P. Martin, J. P. Geindre, and P. Audebert, Opt. Lett. **32**, 310 (2007).
[7]P. Mckenna, F. Lindau, O. Lundh, D. Neely, A. Persson, and C.-G. Wahlstrom, Philos. Trans. R. Soc. A **364**, 711 (2006).
[8]M. Kaluza, J. Schreiber, M. I. K. Santala, G. D. Tsakiris, K. Eidmann, J. Meyer-ter-Vehn, and K. J. Witte, Phys. Rev. Lett. **93**, 045003 (2004).
[9]D. Neely, P. Foster, A. Robinson, F. Lindau, O. Lundh, A. Persson, C.-G. Wahlstrom, and P. McKenna, Appl. Phys. Lett. **89**, 021502 (2006).
[10]P. Antici, J. Fuchs, E. d'Humières, E. Lefebvre, M. Borghesi, E. Brambrink, C. A. Cecchetti, S. Gaillard, L. Romagnani, Y. Sentoku, T. Toncian, O. Willi, P. Audebert, and H. Pépin, Phys. Plasmas **14**, 030701 (2007).
[11]T. Ceccotti, A. Lévy, H. Popescu, F. Réau, P. D'Oliveira, P. Monot, J. P. Geindre, E. Lefebvre, and Ph. Martin, Phys. Rev. Lett. **99**, 185002 (2007).
[12]A. Henig, D. Kiefer, K. Markey, D. C. Gautier, K. A. Flippo, S. Letzring, R. P. Johnson, T. Shimada, L. Yin, B. J. Albright, K. J. Bowers, J. C. Fernández, S. G. Rykovanov, H.-C. Wu, M. Zepf, D. Jung, V. Kh. Liechtenstein, J. Schreiber, D. Habs, and B. M. Hegelich, Phys. Rev. Lett. **103**, 045002 (2009).
[13]A. Lévy, R. Nuter, T. Ceccotti, P. Combis, M. Drouin, L. Gremillet, P. Monot, H. Popescu, F. Réau, E. Lefebvre, and P. Martin, New J. Phys. **11**, 093036 (2009).
[14]S. P. Hatchett, C. G. Brown, T. E. Cowan, E. A. Henry, J. S. Johnson, M. H. Key, J. A. Koch, A. B. Langdon, B. F. Lasinski, R. W. Lee, A. J. Mackinnon, D. M. Pennington, M. D. Perry, T. W. Phillips, M. Roth, T. Craig Sangster, M. S. Singh, R. A. Snavely, M. A. Stoyer, S. C. Wilks, and K. Yasuike, Phys. Plasmas **7**, 2076 (2000).
[15]S. C. Wilks, A. B. Langdon, T. E. Cowan, M. Roth, M. Singh, S. Hatchett, M. H. Key, D. Pennington, A. MacKinnon, and R. A. Snavely, Phys. Plasmas **8**, 542 (2001).
[16]R. A. Loch, A. Lévy, T. Ceccotti, F. Quéré, C. Thaury, H. George, F. Bijkerk, K.-J. Boller, and Ph. Martin, Eur. Phys. J.: Spec. Top. **175**, 133 (2009).
[17]A. Andreev, A. Lévy, T. Ceccotti, C. Thaury, K. Platonov, R. A. Loch, and Ph. Martin, Phys. Rev. Lett. **101**, 155002 (2008).
[18]S. Steinke, A. Henig, M. Schnürer, T. Sokollik, P. V. Nickles, D. Jung, D. Kiefer, R. Hörlein, J. Schreiber, T. Tajima, X. Q. Yan, M. Hegelich, J. Meyer-ter-Vehn, W. Sandner, and D. Habs, Laser Part. Beams **28**, 215 (2010).
[19]R. A. Loch, Ph. Martin, T. Ceccotti, P. Monot, F. Quéré, H. George, M. Bougeard, F. Réau, P. d'Oliveira, and K.-J. Boller, *Laser-Driven Relativistic Plasmas Applied to Science, Industry and Medicine: 2nd International Symposium* (AIP, 2009), Vol. 1153, p. 94.
[20]ACF-Metals, ACF-metals product description and technical information, 2005.
[21]J. O. Stoner, Jr., Nucl. Instrum. Methods Phys. Res., Sect. A **303**, 94 (1991).
[22]A. J. Mackinnon, Y. Sentoku, P. K. Patel, D. W. Price, S. Hatchett, M. H. Key, C. Andersen, R. Snavely, and R. R. Freeman, Phys. Rev. Lett. **88**, 215006 (2002).
[23]Y. Sentoku, T. E. Cowan, A. Kemp, and H. Ruhl, Phys. Plasmas **10**, 2009 (2003).
[24]G. Bonnaud and C. Reisse, Nucl. Fusion **26**, 633 (1986); E. Lefebvre and G. Bonnaud, Phys. Rev. Lett. **74**, 2002 (1995).
[25]P. Gibbon, A. Andreev, E. Lefebvre, G. Bonnaud, H. Ruhl, J. Delettrez, and A. R. Bell, Phys. Plasmas **6**, 947 (1999).
[26]R. A. Loch, "High harmonic generation and ion acceleration with high-intensity laser pulses," Ph.D. thesis, University of Twente, 2009; P. Antici, J. Fuchs, E. d'Humières, J. Robiche, E. Brambrink, S. Atzeni, A. Schiavi, Y. Sentoku, P. Audebert, and H. Pépin, New J. Phys. **11**, 023038 (2009).
[27]C. K. Birdsall and A. B. Langdon, *Plasma Physics via Computer Simulation* (McGraw-Hill, New York, 1985).
[28]E. G. Gamaly, A. V. Rode, and B. Luther-Davies, Appl. Phys. A **69**, S121 (1999).
[29]N. Furstenau, Fresenius Z. Anal. Chem. **308**, 201 (1981).
[30]S. Amoruso, G. Ausanio, M. Vitiello, and X. Wang, Appl. Phys. A **81**, 981 (2005).

[31]E. Matthias, J. Siegel, S. Petzoldt, M. Reichling, H. Skurk, O. Käding, and E. Neske, Thin Solid Films **254**, 139 (1995).
[32]M. E. Povarnitsyn, N. E. Andreev, P. R. Levashov, K. V. Khishchenko, and O. N. Rosmej, Phys. Plasmas **19**, 023110 (2012).
[33]J. P. Colombier, P. Combis, F. Bonneau, R. Le Harzic, and E. Audouard, Phys. Rev. B **71**, 165406 (2005).
[34]J. P. Colombier, P. Combis, A. Rosenfeld, I. V. Hertel, E. Audouard, and R. Stoian, Phys. Rev. B **74**, 224106 (2006).
[35]E. Lefebvre, L. Gremillet, A. Lévy, R. Nuter, P. Antici, M. Carrié, T. Ceccotti, M. Drouin, J. Fuchs, V. Malka, and D. Neely, New J. Phys. **12**, 045017 (2010).
[36]A. Henig, Ph.D. Dissertation (Ludwig–Maximilians–Universität, München, 2010).